Nuclear Engineering and Design 238 (2008) 2285–2291

Contents lists available at ScienceDirect

Nuclear Engineering and Design

journal homepage: www.elsevier.com/locate/nucengdes

Transmission probability method for solving neutron transport equation in three-dimensional triangular-*z* geometry

Guoming Liu*, Hongchun Wu, Liangzhi Cao

Department of Nuclear Engineering, Xi'an Jiaotong University, Xi'an, Shaanxi 710049, China

ARTICLE INFO

Article history:
Received 8 October 2007
Received in revised form 5 March 2008
Accepted 7 March 2008

ABSTRACT

This paper presents a transmission probability method (TPM) to solve the neutron transport equation in three-dimensional triangular-*z* geometry. The source within the mesh is assumed to be spatially uniform and isotropic. At the mesh surface, the constant and the simplified P_1 approximation are invoked for the anisotropic angular flux distribution. Based on this model, a code TPMTDT is encoded. It was verified by three 3D Takeda benchmark problems, in which the first two problems are in *XYZ* geometry and the last one is in hexagonal-*z* geometry, and an unstructured geometry problem. The results of the present method agree well with those of Monte-Carlo calculation method and Spherical Harmonics (P_N) method.

1. Introduction

New concepts and advanced nuclear reactor core design requires solving neutron transport equation on unstructured meshes quickly and efficiently. Some methods, for example, the finite element method (Cao and Wu, 2007), Monte-Carlo method, were well developed for this purpose. But most of finite element methods are coupled with S_N method (Ju et al., 2007) or P_N method (Cao and Wu, 2004), which makes them very complicated and time consuming. So they are effective in shielding calculation, but not suitable for assembly burn up calculation. Monte-Carlo method is a statistical method, which is totally different from deterministic methods. It also requires large computational cost, especially for burn up calculations.

The transmission probability method (TPM) is an efficient tool for the assembly calculation of nuclear reactor. Many worldwide used transport codes, for example, CASMO (Malte and Ake, 1988) and DRAGON (Roy et al., 1994), make use of this method. The geometries of these codes treated with are mostly rectangle (Stepanek et al., 1983; Häggblom et al., 1975) and hexagon meshes (Wasastjerna, 1979; Zhang, 2000) in two dimensions, and the cube and the hexagonal-*z* meshes (Marleau et al., 1990; Garcia, 2003) in three-dimensions, which are all structured meshes. Wu et al. (2007) developed the TPM based on two-dimensional triangular meshes. Numerical results show that this method is very effective for 2D assembly calculation on irregular geometries. But 2D calculation is always not enough if the neutronics/thermo-hydraulics coupling calculation is required to perform the core design because the axial power distribution of an assembly is very crucial for thermo-hydraulics calculation. Thus, it is necessary to develop three-dimensional TPM based on triangular-*z* meshes.

This paper derived the TPM for solving neutron transport equation in three-dimensional triangular-*z* meshes. Unlike the TPM based on triangle meshes (Wu et al., 2007) in two-dimensional geometry, the TPM for triangular-*z* geometry has to treat with axial neutron flux as well as radial neutron flux. The angle of the outgoing interface neutron flux of triangular-*z* meshes is divided into four quadrants compared to two quadrants in triangle meshes in two dimensions. The formula of simplified P_1 approximation of axial neutron flux in each quadrant is different to the formula for radial neutron flux. Moreover, the calculation of leakage probability and transmission probability for triangular-*z* geometry is more complex than the triangle meshes. In triangular-*z* meshes, the discussion of neutron flying for probability calculation depends on not only radial variables but also the axial variables.

The remainder of this paper is organized as follow. The basic equations of the TPM based on the triangular-*z* mesh are derived in Section 2.1. The approximations of the interior neutron source and interface neutron flux are described in Section 2.2. The calculation of the leakage and transmission probabilities is given in Section 2.3. The numerical results for three 3D benchmark problems and an unstructured geometry problem are given in Section 3. Conclusions are summarized in Section 4.

2. Theoretical modal

2.1. Basic equations

Suppose, the 3D calculation region be divided into IE triangular-*z* meshes and suppose the material in each mesh be homogeneous.

* Corresponding author. Tel.: +86 29 82663285.
E-mail address: gmliusy@gmail.com (G. Liu).

0029-5493/$ – see front matter © 2008 Elsevier B.V. All rights reserved.
doi:10.1016/j.nucengdes.2008.03.002

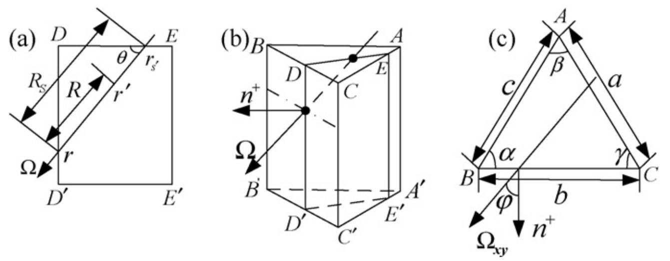

Fig. 1. Neutron flying direction in triangular-*z* mesh.

For each mesh, the neutron integral transport equation is written as:

$$\Phi_g(\vec{r},\vec{\Omega}) = \int_0^{R_s} Q_g(\vec{r}',\vec{\Omega})\,\mathrm{e}^{-\Sigma_{t,g}R}\mathrm{d}R + \Phi_g^-(\vec{r}_{S'},\vec{\Omega})\,\mathrm{e}^{-\Sigma_{t,g}R_s} \qquad (1)$$

where $\Phi_g(\vec{r},\vec{\Omega})$ is the neutron angular flux at $\vec{r}$ in direction $\vec{\Omega}$; $Q_g(\vec{r}',\vec{\Omega})$ is the neutron source at $\vec{r}'$ in direction $\vec{\Omega}$ and $\Phi_g^-(\vec{r}_{S'},\vec{\Omega})$ is the incoming neutron angular flux at $\vec{r}_{S'}$ of surface S'. The integral variable R, which is the length of neutron flying in the triangular-*z* mesh, equals to $|\vec{r}-\vec{r}'|$ and the variable R_S, which is the total length of the neutron flying in this mesh, equals to $|\vec{r}-\vec{r}_{S'}|$. Both R and R_S are shown as in Fig. 1(a). The angles crossed by three side surfaces of triangular-*z* mesh are denoted by α, β and γ, respectively shown in Fig. 1(c).

For clearly, take the side surface BB′CC′ as shown in Fig. 1(b), as example. Set the outward normal $\vec{n}^+$ of the side surface be the basis axes. Denote the angle between the direction $\vec{\Omega}_{xy}$, which is the projection of neutron flight direction $\vec{\Omega}$ on the *X*-*Y* plane, and the normal $\vec{n}^+$ by φ as shown in Fig. 1(c). Denote the angle between $\vec{\Omega}$ and the top surface by θ as shown in Fig. 1(a). Then the direction $\vec{\Omega}$ can be defined by φ and θ.

For convenience, the neutron flying outward direction of this side surface can be divided into four quadrants according to φ and θ. They are denoted by 1, 2, 3, 4 as shown in Fig. 2(a). All quadrants are defined as follows:

- Quadrant 1 (q=1): $0\le\varphi\le\pi/2$, $0\le\theta\le\pi/2$;
- Quadrant 2 (q=2): $-\pi/2\le\varphi\le 0$, $0\le\theta\le\pi/2$;
- Quadrant 3 (q=3): $-\pi/2\le\varphi\le 0$, $-\pi/2\le\theta\le 0$;
- Quadrant 4 (q=4): $0\le\varphi\le\pi/2$, $-\pi/2\le\theta\le 0$.

In each quadrant, the angular flux will be approximated with simplified P_1 approximation in the angle variable and homogeneous in the special variable.

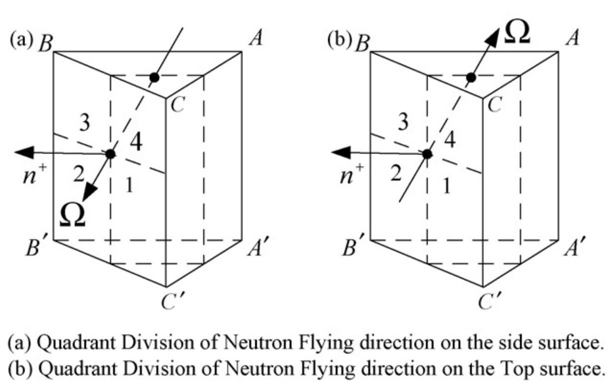

Fig. 2. Quadrant division of the neutron flying direction. (a) Quadrant division of neutron flying direction on the side surface. (b) Quadrant division of neutron flying direction on the top surface.

The flying direction of the outward neutron flux of the top surface and the incoming neutron flux of the side surface is the similar as shown in Fig. 2(b).

For simplicity, denote the three side surfaces, top and bottom surface by 1 (surface BB′CC′), 2 (side surface AA′CC′), 3 (side surface AA′BB′), 4 (top surface ABC), and 5 (bottom surface A′B′C′). In the following, the surface is denoted by k (k = 1–5).

Multiply both sides of Eq. (1) by $\mathrm{d}\vec{\Omega}\mathrm{d}S_k$ and $(\vec{\Omega}\cdot\vec{n}_k^+)\mathrm{d}\vec{\Omega}\mathrm{d}S_k$, respectively, take the integral over the surface k at quadrant q, the outward neutron flux and current are deduced as:

$$\Phi_{k,q}^+ = \int_{S_k}\mathrm{d}S_k\int_q \mathrm{d}\vec{\Omega}\int_0^{R_S} Q(\vec{r}',\vec{\Omega})\,\mathrm{e}^{-\Sigma_t R}\mathrm{d}R + \sum_{\substack{k'\\k'\neq k}}\int_{S_{k'}}\mathrm{d}S_{k'}\int_{q'}\Phi^-(\vec{r}_{k'},\vec{\Omega})\,\mathrm{e}^{-\Sigma_t R_S}\frac{(\vec{\Omega}\cdot n_{k'}^-)}{(\vec{\Omega}\cdot n_k^+)}\mathrm{d}\vec{\Omega} \qquad (2)$$

$$J_{k,q}^+ = \int_{S_k}\mathrm{d}S_k\int_q(\vec{\Omega}\cdot n_k^+)\mathrm{d}\vec{\Omega}\int_0^{R_S} Q(\vec{r}',\vec{\Omega})\,\mathrm{e}^{-\Sigma_t R}\mathrm{d}R + \sum_{\substack{k'\\k'\neq k}}\int_{S_{k'}}\mathrm{d}S_{k'}\int_{q'}\Phi^-(\vec{r}_{k'},\vec{\Omega})\,\mathrm{e}^{-\Sigma_t R_S}(\vec{\Omega}\cdot n_{k'}^-)\mathrm{d}\vec{\Omega} \qquad (3)$$

In each triangular-*z* mesh, the neutron balance equation is

$$\bar{\Phi}_e = \frac{\bar{Q}_e}{\Sigma_{t,e}} - \frac{J_e}{\Sigma_{t,e}V_e} \qquad (4)$$

where V_e is the volume of the triangular-*z* mesh '*e*'; $\bar{\Phi}_e$ is the average flux of the mesh '*e*'; $\Sigma_{t,e}$ is the total cross-section of material in the mesh '*e*'; $\bar{Q}_e$ is the average neutron source of the mesh '*e*' and J_e is the net outward neutron flow through the mesh '*e*' boundaries. Eqs. (2)–(4) are the basic equations of the TPM based on the triangular-*z* mesh.

2.2. Approximation

The interior source within a triangular-*z* mesh is assumed to be constant in spatial distribution and isotropic in angular distribution. The surface neutron angular flux of each quadrant is approximated with simplified P_1 approximation in the angle variable and homogeneous in the special variable. The neutron angular flux distribution of the side surface k at quadrant q is expanded as

$$\Phi_{k,q}(\vec{r}_s,\vec{\Omega}) = \frac{1}{4\pi}[f_{k,q}^{(00)} + 3f_{k,q}^{(10)}\cos\theta\cos\varphi] \qquad (5)$$

The neutron angular flux distribution of the top and bottom surface is expanded as

$$\Phi_{k,q}(\vec{r}_s,\vec{\Omega}) = \frac{1}{4\pi}[f_{k,q}^{(00)} + 3f_{k,q}^{(10)}\sin\theta] \qquad (6)$$

where $f_{k,q}^{(00)}$ and $f_{k,q}^{(10)}$ are the expansion coefficients. The expression of the expansion coefficients can be deduced as

$$f_{k,q}^{(00)} = \frac{8(2\Phi_{k,q}^+ - 3J_{k,q}^+)}{S_k} \qquad (7)$$

$$f_{k,q}^{(10)} = \frac{8(2J_{k,q}^+ - \Phi_{k,q}^+)}{S_k} \qquad (8)$$

2.3. Probability calculation

Substituting Eqs. (5)–(8) into Eq. (2) and Eq. (3), respectively, the outward neutron flux and current are expressed as

$$\Phi^+_{k,q} = V_e\bar{Q}_e E^{(0)}_{k,q} + \sum_{k'\neq k}[(8T^{(00)}_{k',k} - 12T^{(10)}_{k',k})\Phi^+_{k',q'} + (24T^{(10)}_{k',k} - 12T^{(00)}_{k',k})J^+_{k',q'}] \tag{9}$$

$$J^+_{k,q} = V_e\bar{Q}_e E^{(1)}_{k,q} + \sum_{k'\neq k}[(8T^{(01)}_{k',k} - 12T^{(11)}_{k',k})\Phi^+_{k',q'} + (24T^{(11)}_{k',k} - 12T^{(01)}_{k',k})J^+_{k',q'}] \tag{10}$$

where $E^{(l)}_{k,q}$ is the leakage probability of the surface k at quadrant q and $T^{(l'l)}_{k',k}$ is the transmission probability from surface k' to k. The superscripts (0) and (1) denote the neutron flux and the neutron current. The superscripts (0 0), (0 1), (1 0), (1 1) indicate the transmission of flux to flux, flux to current, current to flux and current to current, respectively. The probability formulae can be derived as

$$E^{(l)}_{k,q} = \frac{1}{4\pi V_e}\int_{s_k}\int_{q}\int_0^{R_S}(\bar{\Omega}\cdot\vec{n}^+_k)^l\,\mathrm{e}^{-\Sigma_t R}\mathrm{d}R\mathrm{d}\bar{\Omega}\mathrm{d}S_k \tag{11}$$

$$T^{l'l}_{k'k} = \frac{1}{\pi S_{k'}}\int_{S_{k'}}\int_{q'}\frac{(\bar{\Omega}\cdot\vec{n}^-_{k'})^{(1+l')}}{(\bar{\Omega}\cdot\vec{n}^+_k)^{(1-l)}}\,\mathrm{e}^{-\Sigma_t R_S}\mathrm{d}\bar{\Omega}\mathrm{d}S_{k'} \tag{12}$$

It can be seen from the Eq. (11) that the calculations of leakage probability are integrals about the angular ($\mathrm{d}\bar{\Omega} = \cos\theta\mathrm{d}\theta d\varphi$), the surface area ($\mathrm{d}S$ or $\mathrm{d}S_{k'}$) and the length of neutron flying in the triangular-z mesh ($\mathrm{d}R$). The limits of the integral variable are different depend on what the type of neutron flying in the triangular-z mesh is. There are four types of neutron flying in the mesh: flying from the top surface to the side surface, flying from the top surface to the bottom surface, flying from the side surface to the side surface and flying from the side surface to the top surface. The probability calculation is similar for the four types. For simplicity, we only take the type of neutron flying from the side surface to the side surface as example for discussion. In this type, the probability formulae can be expanded as

$$E^{(l)}_{k,q} = \frac{1}{4\pi S_k}\int_{\varphi_-}^{\varphi_+}\int_{s_-}^{s_+}\int_{h_-}^{h_+}\int_{\theta_-}^{\theta_+}\int_0^{R_S}\cos^l\varphi\cos^l\theta\,\mathrm{e}^{-\Sigma_t R}\mathrm{d}R\mathrm{d}\theta\mathrm{d}h\mathrm{d}s\mathrm{d}\varphi \tag{13}$$

$$T^{l'l}_{k'k,q'q} = \frac{1}{\pi S_{k'}}\int_{\varphi_-}^{\varphi_+}\int_{s_-}^{s_+}\int_{\theta_-}^{\theta_+}\int_{h_-}^{h_+}\cos^l\varphi\cos^{1+l+l'}\theta\,\mathrm{e}^{-\Sigma_t R_S}\mathrm{d}h\mathrm{d}\theta\mathrm{d}s\mathrm{d}\varphi \tag{14}$$

2.3.1. Leakage probability calculation

The leakage probability of each side surface at each quadrant contains many complex cases. Take an example; the leakage probability of the surface 1 quadrant 1 includes two contributions. One is neutron flying from surface 2 to surface 1 quadrant 1 as shown in Fig. 3(a). The other one is from surface 3 to surface 1 quadrant 1. Because of the difference of integral limits of variable φ and s, the second part consists of two different cases as shown in Fig. 3(b) and (c).

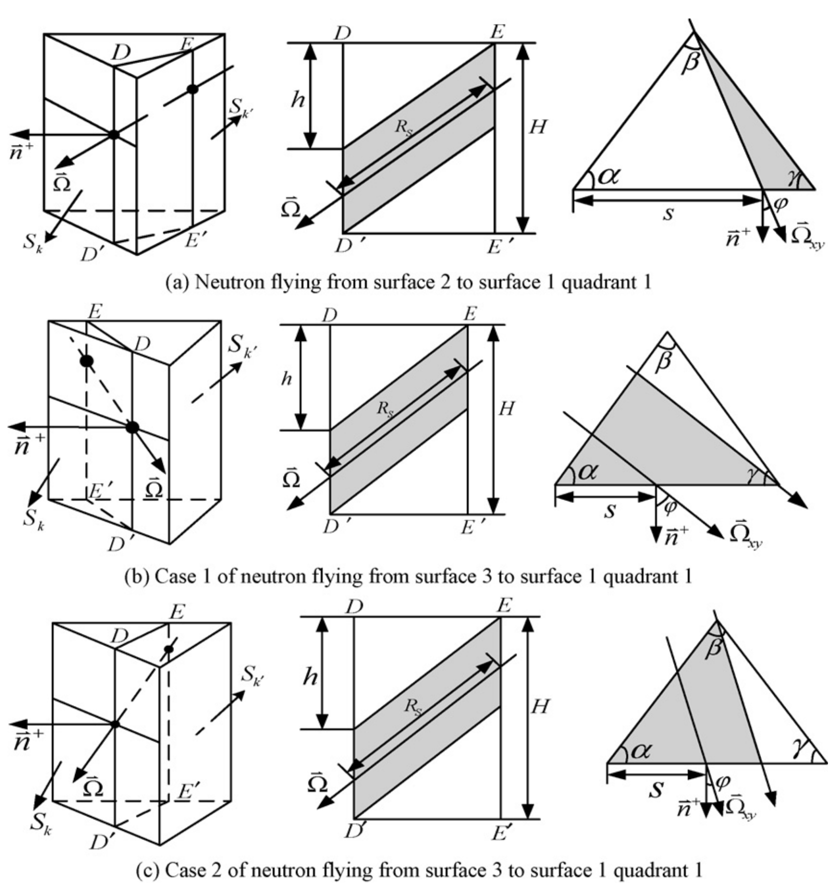

Fig. 3. Leakage probability calculation of surface 1 quadrant 1. (a) Case 1 of neutron flying from surface 3 to surface 1 quadrant. (b) Case 2 of neutron flying from surface 3 to surface 1 quadrant 1. (c) Neutron flying from surface 2 to surface 1 quadrant 1.

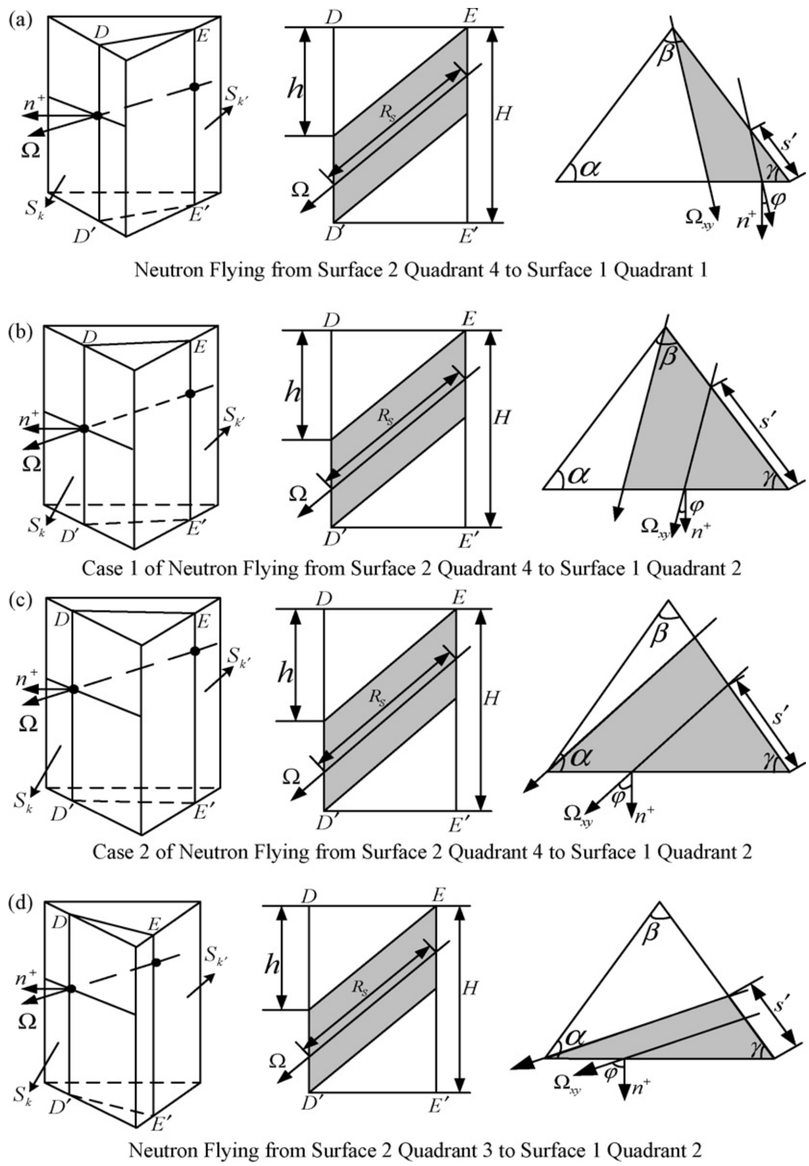

Fig. 4. Transmission probability calculation of neutron flying from surface 2 to surface 1. (a) Neutron flying from surface 2 quadrant 4 to surface 1 quadrant 1. (b) Case 1 of neutron flying from surface 2 quadrant 4 to surface 1 quadrant 2. (c) Case 2 of neutron flying from surface 2 quadrant 4 to surface 1 quadrant 2. (d) Neutron flying from surface 2 quadrant 3 to surface 1 quadrant 2.

The limits of the above three cases are as follows:

(1) $\theta \in [0, \ (\pi/2)-\gamma]$, $s \in [0, \ c\cos(\varphi-\alpha)/\cos\varphi]$, $h \in [l_0 \tan\theta, \ \mathrm{H}]$, $\theta \in [-\arctan(H/l_0), 0]$;
(2) $\varphi \in [(\pi/2)-\gamma, \pi/2]$, $s \in [0, b]$, $h \in [l_0 \tan\theta, \mathrm{H}]$, $\theta \in [-\arctan(H/l_0), 0]$;
(3) $\varphi \in [0, \ (\pi/2)-\gamma]$, $s \in [b-(a\cos(\varphi-\gamma))/\cos\varphi, \ b]$, $h \in [l_0 \tan\theta, \ \mathrm{H}]$, $\theta \in [-\arctan(H/l_0), 0]$;

and $R_S = l_0/\cos\theta$.

Substitute the above expressions into the integral variables and limits in Eq. (13), the total leakage probability of the surface 1 quad-

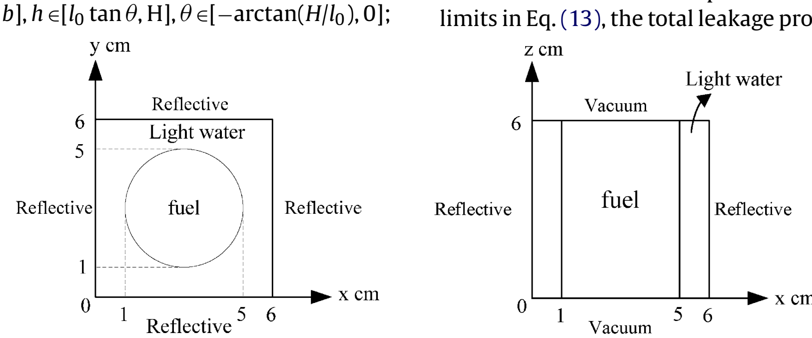

Fig. 5. Configuration of problem 4.

Table 1
Comparison of K_{eff} and control rod worth for problem 1

Method	Case 1	Case 2	CR-worth
Monte-Carlo	0.9732	0.9594	1.47E−02
MARK/P_N	+0.637[a]	+0.553	+6.12
TPMTDT	+0.435	+0.462	−2.04

[a] Relative differences from Monte-Carlo (%).

rant 1 is:

$$E_{1,1}^{(l)} = \frac{1}{4\pi\Sigma_t bH}\left[\int_{(\pi/2)-\gamma}^{\pi/2}\int_0^b\int_{-\arctan(H/l_0)}^{0} A\mathrm{d}\theta\mathrm{d}s\mathrm{d}\varphi + \int_0^{(\pi/2)-\gamma}\int_0^{c(\cos(\varphi-\alpha)/\cos\varphi)}\int_{-\arctan(H/l_0)}^{0} A\mathrm{d}\theta\mathrm{d}s\mathrm{d}\varphi + \int_0^{(\pi/2)-\gamma}\int_{b-a(\cos(\varphi+\gamma)/\cos\varphi)}^{b}\int_{-\arctan(H/l_0)}^{0} A\mathrm{d}\theta\mathrm{d}s\mathrm{d}\varphi\right] \quad (15)$$

where the expression of l_0 is $s\sin\alpha/\cos(\varphi-\alpha)$ and the expression of the integral function A is $\cos^l\varphi\cos^{l+1}\theta(1-\mathrm{e}^{-\Sigma_t l_0/\cos\theta})(H-l_0\tan\theta)$.

2.3.2. *Transmission probability calculation*

The transmission probability form a side surface to the other side surface also contains many complex cases. Take an example, the transmission probability of the side surface 2 to the side surface1 consists of three parts, they are neutron flying from surface 2 quadrant 4 to surface 1 quadrant 1, neutron flying from surface 2 quadrant 4 to surface 1 quadrant 2, which part contains two different cases, and neutron flying from surface 2 quadrant 3 to surface 1 quadrant 2. These four cases are shown in Fig. 4(a)–(d), respectively.

The limits of integral variables corresponding to above four cases are as follows:

(1) $\theta\in[0,(\pi/2)-\gamma]$, $s'\in[0,a]$, $h\in[l_0\tan\theta, \mathrm{H}]$, $\theta\in[-\arctan(H/l_0),0]$;
(2) $\varphi\in[\alpha-(\pi/2),0]$, $s'\in[0,a]$, $h\in[l_0\tan\theta, \mathrm{H}]$, $\theta\in[-\arctan(H/l_0),0]$;
(3) $\varphi\in[-\gamma,\ \alpha-(\pi/2)]$, $s'\in[0,\ b\cos\varphi/\cos(\varphi+\gamma)]$, $h\in[l_0\tan\theta,\ \mathrm{H}]$, $\theta\in[-\arctan(H/l_0),0]$;
(4) $\varphi\in[-\pi/2,\ -\gamma)]$, $s'\in[0,\ b\cos\varphi/\cos(\varphi+\gamma)]$, $h\in[l_0\tan\theta,\ \mathrm{H}]$, $\theta\in[-\arctan(H/l_0),0]$;

and $R_S = l_0/\cos\theta$.

Substitute the above expressions into the integral variables and limits in Eq. (14), the expression of transmission probability corresponding to the four cases of neutron flying from the surface 2 to surface 1 is:

$$T_{21,41}^{(l'l)} = \frac{1}{\pi aH}\int_0^{(\pi/2)-\gamma}\int_0^a\int_{-\arctan(H/l_0)}^{0} B\mathrm{d}\theta\mathrm{d}s'\mathrm{d}\varphi \quad (16)$$

$$T_{21,42}^{(l'l)} = \frac{1}{\pi aH}\int_{\alpha-(\pi/2)}^{0}\int_0^a\int_{-\arctan(H/l_0)}^{0} B\mathrm{d}\theta\mathrm{d}s'\mathrm{d}\varphi + \int_{-\gamma}^{\alpha-(\pi/2)}\int_0^{b\cos\varphi/\cos(\varphi+\gamma)}\int_{-\arctan(H/l_0)}^{0} B\mathrm{d}\theta\mathrm{d}s'\mathrm{d}\varphi \quad (17)$$

$$T_{21,32}^{(l'l)} = \frac{1}{\pi aH}\int_{-\pi/2}^{-\gamma}\int_0^{b\cos\varphi/\cos(\varphi+\gamma)}\int_{-\arctan(H/l_0)}^{0} B\mathrm{d}\theta\mathrm{d}s'\mathrm{d}\varphi \quad (18)$$

where the expression of l_0 is $s\sin\alpha/\cos(\varphi-\alpha)$ and the expression of the integral function B is $\cos^{l-1}\varphi\cos^{l'+1}(\varphi+\gamma)\cos^{l+1}\theta(1-\mathrm{e}^{-\Sigma_t l_0/\cos\theta})(H-l_0\tan\theta)$.

3. Numerical results

The code TPMTDT was developed based on the TPM method described above. Three 3D Takeda benchmark problems, which are, a small FBR core, an axially heterogeneous FBR core (which both are in *XYZ* geometry), and a small FBR core with hexagonal-*z* geometry, and an unstructured geometry problem were calculated. The reference value of the three 3D Takeda benchmark problems is the average calculations of Monte-Carlo method and P_N method contributed to the benchmark, which was computed by the variance weighted procedure (Takeda and Ikeda, 1991a, b). The reference value of the unstructured geometry problem is the calculation results of MG-MCNP3B code.

Table 2
Region averaged group fluxes for rod-in case of problem 1

Method		Core	Axial blanket	Control rod
Monte-Carlo	1G	4.3482E−05	5.2029E−06	1.6556E−05
	2G	2.4171E−04	4.6772E−05	9.1050E−05
	3G	1.6200E−04	4.6190E−05	5.1815E−05
	4G	6.0438E−06	3.6287E−06	1.1073E−06
MARK/P_N	1G	−1.741[a]	+5.7564	+111.6
	2G	−1.187	+11.63	+106.7
	3G	−0.040	+27.27	+102.7
	4G	+0.822	−0.1102	+90.68
TPMTDT	1G	+3.402	−6.091	+15.71
	2G	+2.064	+1.780	+10.58
	3G	−2.765	−8.257	+12.37
	4G	−2.839	+1.530	+16.73

[a] Relative differences from Monte-Carlo (%).

Table 3
Comparison of K_{eff} and control rod worth for problem 2

Method	Case 1	Case 2	Case 3	CR-worth	CRP-worth
Monte-Carlo	0.9709	1.0005	1.0214	3.05E−02	2.03E−02
EVENT (P_5)	+0.632[a]	+0.3498	+0.3234	−10.16	−0.9852
TPMTDT	+0.453	+0.3298	+0.2937	−4.590	−1.477

[a] Relative differences from Monte-Carlo (%).

Table 4
Region averaged group fluxes for case 3 of problem 2

Method		Core	Internal blanket	Radial blanket	Axial blanket
Monte-Carlo	1G	1.9033E−05	1.1875E−05	1.3718E−06	2.7276E−06
	2G	1.1026E−04	1.0838E−04	1.4703E−05	2.8409E−05
	3G	8.0177E−05	1.1672E−04	1.9121E−05	3.3614E−05
	4G	3.1958E−06	7.0366E−06	1.6164E−06	3.5169E−06
EVENT (P_5)	1G	+2.196[a]	+3.377	+3.076	+4.436
	2G	+2.295	+2.316	+2.374	+2.837
	3G	+2.388	+2.245	+2.348	+2.719
	4G	+2.200	+2.447	+1.590	+4.026
TPMTDT	1G	+4.067	+4.391	−2.668	+2.896
	2G	+3.918	−2.316	+4.720	+2.460
	3G	+3.282	−5.541	−1.475	+1.276
	4G	+2.547	−2.116	+3.718	+2.198

[a] Relative differences from Monte-Carlo (%).

Table 5
Comparison of K_{eff} and control rod worth for problem 3

Method	Case 1	Case 2	Case 3	CR-worth
Monte-Carlo	1.0951	0.9833	0.8799	2.23E−01
MARK/P_N	−0.082[a]	0.010	0.2273	−1.345
TPMTDT	+0.237	0.3356	0.1818	−3.139

[a] Relative differences from Monte-Carlo (%).

Table 6
Region averaged group fluxes for case 3 of problem 3

Method		Test zone	Axial blanket	Driver with moderator	Control rod
Monte-Carlo	1G	1.4695E−04	3.7122E−05	7.0291E−05	4.4354E−05
	2G	1.1251E−04	4.8758E−05	5.1347E−05	3.5773E−05
	3G	2.6560E−05	2.2353E−05	3.6997E−05	7.7894E−06
	4G	2.4518E−06	8.6671E−06	1.3952E−05	4.8143E−07
MARK/P_N	1G	−0.5172[a]	+8.165	−1.510	+3.341
	2G	−0.4355	+6.018	−1.986	+1.409
	3G	+0.6212	+5.521	−25.40	+60.94
	4G	+6.077	+6.179	+0.1218	+702.4
TPMTDT	1G	+4.797	+8.217	−2.195	+3.756
	2G	+2.524	+4.080	−3.110	+4.629
	3G	+3.618	+5.891	−11.69	+10.04
	4G	+3.145	+5.303	−1.927	+26.36

[a] Relative differences from Monte-Carlo (%).

Table 7
Cross sections of unstructured geometry problem

Group	Region	$\gamma\Sigma_f$	$\Sigma_{S,g\to1}$	$\Sigma_{S,g\to2}$	Σ_t
1 (fast neutron)	Fuel	6.203E−03	1.780E−01	1.002E−02	1.9665E−01
	Water	0.0	1.995E−01	2.188E−02	2.2206E−01
2 (thermal neutron)	Fuel	1.101E−01	1.089E−03	5.255E−01	5.9616E−01
	Water	0.0	1.558E−03	8.783E−01	8.8787E−01

3.1. Small FBR core

This is a small core model of a FBR. There are two cases. Case 1: the control rod is withdrawn (the control rod position is filled with Na). Case 2: the control rod is half-inserted. The axial mesh size is 4.0 cm. The K_{eff} of the two cases as well as the control rod worth are listed in Table 1. It can be found that the eigenvalues of the TPMTDT agree well with those of the Monte-Carlo method and P_N method. Their differences are less than 0.5%. Table 2 shows the region averaged group fluxes for rod-in case. It can be seen that TPMTDT also agrees well with the Monte-Carlo. It is much better than MARK/P_N in the control rod region.

3.2. Axially heterogeneous FBR core

In this problem, the core has an internal blanket region. There are three cases:

Case 1: the control rods are inserted.
Case 2: the control rods are withdrawn.
Case 3: the control rods are replaced with core or blanket cells.

The axial mesh size is chosen as 5.0 cm for case 1 and case 2, and 4.0 cm for case 3. The k_{eff} of three cases and the associated control rod worth are listed in Table 3. As shown, the eigenvalues of the TPMTDT agree well with those of the Monte-Carlo method with the differences being less than 0.46%. The region averaged group fluxes for case 3 are listed in Table 4. It can be seen the differences in the region averaged group fluxes are less than 5.0% except for the third group in the internal blanket.

3.3. Small FBR core with hexagonal-z geometry

It is a hexagonal-*z* geometry problem with the vacuum boundary conditions. There are three cases:

Case 1: the control rods are withdrawn.
Case 2: the control rods are half-inserted.
Case 3: the control rods are fully inserted.

The axial mesh size is chosen as 4.0 cm for case 1, and 3.75 cm for case 2 and case 3. The k_{eff} of three cases and the associated control rod worth are listed in Table 5. The eigenvalues of the TPMTDT agree well with those of the Monte-Carlo method with the differences being less than 0.4%. The region averaged group fluxes for case 3 are shown in Table 6. It can be found, the averaged flux of TPMTDT agrees no so well with the Monte-Carlo method. However, it is the same level compare with the P_N method.

3.4. Unstructured geometry problem

Through the above results comparison, it is validated that the TPMTD code agrees well with other codes or reference. But all the above problems can use the cube mesh method or hexagon-*z* mesh method to solve. In order to validate the adaptability of TPMTD to calculate the three-dimensional unstructured geometry, a three-dimensional problem with unstructured geometry was developed. It contains a fuel rod surrounded by the light water as shown in Fig. 5. The cross sections are given in Table 7. Table 8 shows the results obtained by the MG-MCNP3B code and the TPMTD code. It shows that the result of the TPMTD code agrees well with the results of MG-MCNP3B code.

Table 8
Results of unstructured geometry problem

Method	The fluxes of fast neutron		The fluxes of thermal neutron		k_{eff}
	Fuel	Water	Fuel	Water	
MG-MCNP3B	1.0[a]	1.198	7.845	5.233	0.07511
TPMTD	1.0	1.158	8.164	5.503	0.07515

[a] Normalization: the fast flux in fuel zone is 1.0.

4. Conclusion

A transmission probability method based on triangular-z mesh for calculating three-dimensional neutron transport equation is developed. The code TPMTDT is verified with three 3D Takeda benchmark problems and the unstructured geometry problem. The differences in k_{eff} between the TPMTDT and the reference are less than 0.5% for all benchmarks. Sometimes the flux in the control rod region is not so good. But it is better than that of the P_{N} method. For improving, the interior source should be approximated with higher order polynomial. This work is under the way.

Acknowledgement

This work is supported by National Natural Science Foundation of China Grants No. 10475064 and No. 10605017.

References

Cao, L.Z., Wu, H.C., 2004. Spherical harmonics method for neutron transport equation based on unstructured-meshes. Nucl. Sci. Tech. 15 (6), 335–339.

Cao, L.Z., Wu, H.C., 2007. A spherical harmonics-Finite element discretization of the self-adjoint angular flux neutron transport equation. Nucl. Eng. Des. 237, 2232–2239.

Garcia, R.D.M., 2003. A numerical method for computing collision, escape, and transmission probabilities in three dimensions. Nucl. Sci. Eng. 144, 200–210.

Häggblom, H., et al., 1975. Transmission probability method of integral neutron transport calculation for two-dimensional rectangular cells. Nucl. Sci. Eng. 156, 411–433.

Ju, H.T., Wu, H.C., Zhou, Y.Q., et al., 2007. A least-squares finite-element S_{N} method for solving first-order neutron transport equation. Nucl. Eng. Des. 237, 823–829.

Malte, E., Ake, A., 1988. CASMO-3: new features, benchmarking, and advanced applications. Nucl. Sci. Eng. 100, 342–351.

Marleau, G., Roy, R., Hebert, A., 1990. Analytic reductions for transmission and leakage probabilities in finite tubes and hexahedra. Nucl. Sci. Eng. 104, 209–216.

Roy, R., Marleau, G., Tajmouati, J., Rozon, D., 1994. Modeling of CANDU reactivity control devices with the lattice code DRAGON. Ann. Nucl. Energy 111, 257–270.

Stepanek, J., Auerbach, T., Haelg, W., 1983. Calculation of four thermal reactor benchmark problems in *X–Y* geometry. EPRI NP-2855.

Takeda, T., Ikeda, H., 1991a. 3D neutron transport benchmarks. J. Nucl. Sci. Technol. 28 (7), 656–669.

Takeda, T., Ikeda, H., 1991b. 3D neutron transport benchmarks, Technical Report OECD/NEA, Committee on Reactor Physics (NEACRP), OSAKA University, NEACRP-L-330.

Wasastjerna, Frej, 1979. Application of the transmission probability method to the calculation of neutron flux distribution in hexagonal geometry. Nucl. Sci. Eng. 172, 9–18.

Wu, H.C., Liu, P.P., Zhou, Y.Q., et al., 2007. Transmission probability method based on triangle meshes for solving unstructured geometry neutron transport problem. Nucl. Eng. Des. 237, 28–37.

Zhang, Y., 2000. Numerical Solution of Two-Dimensional Neutron Integral Transport Equation for Hexagonal Geometry and Development of Software Package for Calculation of PWR Hexagonal Assembly. Xi'an Jiaotong Univerity, Xi'an [D in Chinese].